Available online at www.sciencedirect.com
SCIENCE DIRECT®
Journal of Organometallic Chemistry 689 (2004) 631–638
Journal of Organometallic Chemistry
www.elsevier.com/locate/jorganchem

Acid-base and counter ion dependent solid-state assembly of a ferrocene β-aminoalcohol and the corresponding ammonium salt

Petr Štěpnička [a,*], Ivana Císařová [a], Jiří Ludvík [b]

[a] Department of Inorganic Chemistry, Faculty of Science, Charles University, Hlavova 2030, 128 40 Prague 2, Czech Republic
[b] J. Heyrovský Institute of Physical Chemistry, Academy of Sciences of the Czech Republic, Dolejškova 3, 182 23 Prague 8, Czech Republic

Received 15 July 2003; accepted 29 September 2003

Abstract

2-(Ferrocenylmethyl)amino-2-methylpropan-1-ol was synthesized and converted to the respective ammonium bromide ([**1**H]Br ≡ **2**) and dihydrogenphosphate ([**1**H]H_2PO_4 ≡ **3**). The solid-state structures of **1**, **2** and the solvated salt **3** · 1/6Et_2O (**3a**) have been determined by X-ray diffraction. The solid-state assemblies of **1** and **2** are dominated by infinite ladder-like arrays interconnected by hydrogen bonds whereas the solid-state structure of **3a** is built up from linear hydrogen-bonded dihydrogenphosphate chains, which are interlinked via hydrogen bonds to the cations $[\mathbf{1}H]^+$ into a complicated three-dimensional network. Compound **1** and its interactions with Bu_4NBr and $Bu_4NH_2PO_4$ in solution were further studied by electrochemical methods and NMR titrations.

Keywords: Ferrocene; Aminoalcohols; Hydrogen bonding; X-ray diffraction; Supramolecular assembly; NMR spectroscopy; Electrochemistry

1. Introduction

Crystal engineering with organometallic and coordination compounds is currently gaining attention as an approach towards preparation of new materials whose properties arise from a defined, periodic *and* specific assembly of molecules and ions in the solid state. Organometallic materials are particularly interesting due to a possibility of changing the molecular structure and charge of suitable building blocks, as well as oxidation and spin states of their central atom(s) [1]. The design of organometallic crystals is still far from rational and usually relies on an assembly of polar molecules via hydrogen bonds [2], which are strong enough to ensure stability of the formed supramolecular structures, and better predictable and reproducible due to their directional nature than, e.g., weaker C–H···X and C–H···π interactions frequently encountered in the structures of organometallic compounds.

It has been shown that ferrocenylalcohols form various hydrogen-bonded arrays in the solid state made up of either only the hydroxy groups or involving another polar group present in the molecule [3]. They also readily incorporate other molecules capable of hydrogen bonding, typically amines, into their structures, affording well-defined solid adducts with diverse supramolecular structures [4]. Considering that an introduction of further polar groups increases the number of possible intermolecular interactions, we studied a readily available ferrocene β-aminoalcohol, 2-(ferrocenylmethyl)-amino-2-methylpropan-1-ol (**1**), which appears as a suitable building block for solid-state self-assembly and possibly also for hydrogen bonding-aided intermolecular association/ion recognition. In this paper, we describe the solid-state structures of **1**, ammonium salts [**1**H]Br and [**1**H]H_2PO_4 and, additionally, report on interactions of **1** with Bu_4NBr and $Bu_4NH_2PO_4$ in solution, which were studied by NMR titrations and electrochemical methods.

2. Results and discussion

2-(Ferrocenylmethyl)amino-2-methylpropan-1-ol, $FcCH_2NHCMe_2CH_2OH$ (**1**, Fc = ferrocenyl) was obtained similarly to 2-[(ferrocenylmethyl)amino]ethan-

* Corresponding author.
E-mail address: stepnic@natur.cuni.cz (P. Štěpnička).

0022-328X/$ - see front matter © 2003 Elsevier B.V. All rights reserved.
doi:10.1016/j.jorganchem.2003.11.017

1-ol [5] by condensation of ferrocenecarboxaldehyde with 2-amino-2-methylpropan-1-ol and a subsequent reduction of the intermediate Schiff base (72% isolated yield). The amination reaction competes with the direct reduction of the aldehyde to ferrocenylmethanol, which was isolated as a minor byproduct (10%) [6]. Compound **1** was characterized by NMR, MS and IR spectra, by elemental analysis and further converted to the respective ammonium bromide (**2**) and dihydrogenphosphate (**3**) by neutralization with one-molar equivalent of the respective acid.

As it is almost impossible to elucidate solid-state structure of molecular systems having a number of potential hydrogen bond donor and acceptor groups from only spectral data, we have studied the solid-state structures of **1**, and the salts **2** and **3**. Single crystals of **1** were obtained easily by recrystallization from methanol while microcrystalline bromide **2** separated directly from the mixture during NMR titration (see below). On the other hand, phosphate **3**, which is insoluble in common organic solvents (chloroform, methylene chloride, diethyl ether, hydrocarbons) but well soluble in polar solvents such as methanol, dimethylsulfoxide and water, does not crystallize willingly. X-ray quality crystals were grown by gas-phase diffusion of diethyl ether into a methanol solution of **3** over several weeks. The separated yellow, *very* fine needles were, however, characterized as the solvate $\mathbf{3} \cdot 1/6Et_2O$ (**3a**). Repeated attempts at obtaining defined adducts $\mathbf{1} \cdot x Bu_4NH_2PO_4$ failed; the co-crystallization by diffusion of diethyl ether vapors into mixed **1**-$Bu_4NH_2PO_4$ solutions in acetonitrile (1:1 and 1:2 molar ratios) recovered only colorless needles of pure $Bu_4NH_2PO_4$.

2.1. Solid-state structure of *1*

A view of the molecular structure of **1** is shown in Fig. 1 and the selected geometric parameters are given in Table 1. The arrangement of the ferrocene unit is regular, showing only a negligible tilt of its cyclopentadienyl rings (the unsubstituted cyclopentadienyl ring exhibits a disorder, see Section 4). The geometry of the aminoalcohol side chain corresponds well to analogous ferrocene amines $FcCH_2NHPh$ [7], and $FcCH_2NHCH_2$-(p-C_6H_4Me) [5]. Similarly to the former compound, the arrangement of the substituents at the C11–N bond in **1** is very close to *anti*-periplanar.

The number of classical (OH, NH) hydrogen bond donors in the molecule of **1** perfectly matches the number of the acceptors (hydroxy and amino groups). In the crystal, all these groups participate in hydrogen bonding such that the hydroxy and amino groups act as both the hydrogen bond donors and acceptors to form a linear infinite array running along the crystallographic *a* axis (Fig. 2). Each molecule in the structure of **1** is linked to three neighbors by two pairs of OH···N and NH···O hydrogen bonds: the stronger (shorter) hydrogen bonds O–H(92)···N^{i} [O–H(92) 0.899(2), O···N^{i} 2.925(3) Å, O–H(92)···N^{i} 178.6(2)°; (i) $(x-1, y, z)$] are responsible for linear propagation of the molecular chains whilst the weaker (longer) N–H(91)···O^{ii} bonds [N–H(91) 0.88(3), N···O^{ii} 3.147(3) Å, N–H(91)···O^{ii} 157(2)°; (ii) $(1-x, -y, 2-z)$] cross-link the chains formed from molecules lying across the crystallographic inversion centers to constitute a folded ladder assembly with alternating centrosymmetric cycles of four and eight non-hydrogen atoms. In some regards, the structure of **1**

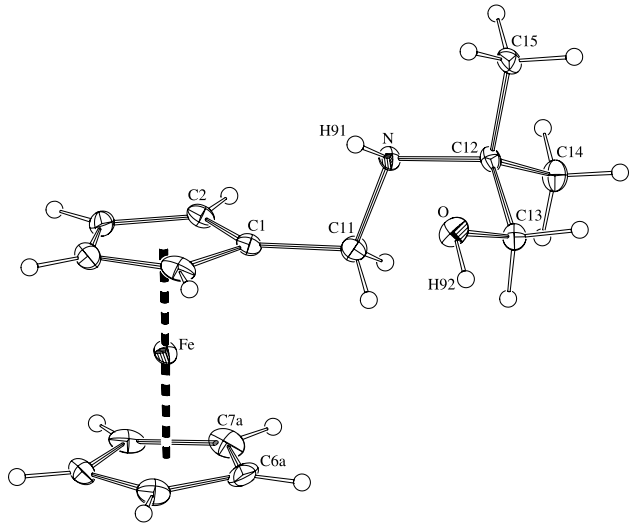

Fig. 1. The molecular structure of aminoalcohol **1** showing the atom labelling scheme. The cyclopentadienyl ring atoms are numbered consecutively and, hence, only pivot and adjacent carbon atoms are labelled. For clarity, only one position of the disordered cyclopentadienyl ring is shown (0.60 occupancy, see Section 4). Thermal motion ellipsoids are drawn at the 30% probability level.

Table 1
The selected structural parameters for **1** and **2** (in Å and °)[a]

Compound	**1**	**2**
Fe–Cg1	1.653(1)	1.643(1)
Fe–Cg2	1.6630(7) [1.6442(7)][b]	1.648(1)
C(1)–C(11)	1.497(4)	1.487(4)
C(11)–N	1.475(3)	1.507(4)
N–C(12)	1.485(3)	1.521(4)
C(12)–C(13)	1.537(3)	1.520(3)
C(13)–O	1.415(3)	1.416(4)
∠Cp1,Cp2	0.9(1) [1.1(1)][b]	2.1(2)
C(1)–C(11)–N	110.6(2)	111.7(2)
C(11)–N–C(12)	115.1(2)	117.5(2)
N–C(12)–C(13)	113.9(2)	109.3(2)
C(12)–C(13)–O	111.3(2)	111.3(2)
C(1)–C(11)–N–C(12)	−172.1(2)	156.8(2)

[a] The ring planes are defined as follows: Cp1, C(1–5); Cp2, C(6–10). Two components for Cp2 in **1** due to a disordered: C(6A–10A) (60%) and C(6B–10B) (40%). Cg denotes the respective ring centroid.
[b] Parameters for cyclopentadienyl rings C(6A–10A) [C(6B–10B)].

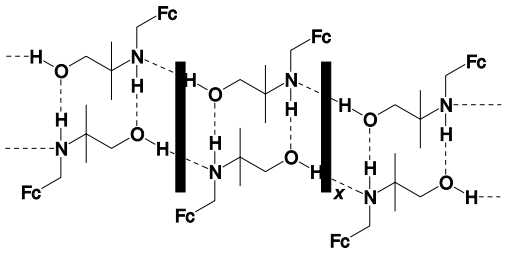

Fig. 2. A schematic drawing of the ladder-like assembly in the structure of **1**.

resembles the solid-state packing of 2-aminoethanol, where the individual molecules associate into infinite chains via relatively stronger NH···O bonds (2.758(3) Å) and, further, by longer NH···O and OH···N (3.183(3) and 3.282(3) Å) bonds into a complicated three-dimensional network [8].

2.2. Solid-state structure of *2*

Upon comparing the structural data of **2** with **1** (Table 1), it is apparent that *N*-protonation of **1** influences the overall geometry only slightly: in accordance with a lower electron density at the nitrogen atom, the C–N bonds are slightly elongated (relatively by about 2%). Additionally, the conformation of the β-hydroxyamine side chain is changed (cf. torsional angles at the $FcCH_2$–N bond), reflecting most likely a different nature of the solid-state interactions.

The three hydrogen atoms at nitrogen (NH_2^+) and oxygen (OH) atoms in **2** are involved in hydrogen bonding to three different bromide ions to form centrosymmetric double chains of alternating $[\mathbf{1}H]^+$ and Br^- ions. The chain components are mutually shifted by the half of the period along the propagation vector parallel to the crystallographic *a* axis (Fig. 3): N–H(91)···Br^{iii} [N···Br^{iii} 3.321(2) Å; (iii) $(1+x, y, z)$], N–H(92)···Br^{iv} [N···Br^{iv} 3.362(2) Å; (iv) $(1-x, 1-y, -z)$], and O–H(93)···Br [O···Br 3.250(2) Å]. The solid-state packing can thus be described as a linear assembly of centrosymmetric four ($\{NH_2Br\}_2$) and ten-membered ($\{NHCCOHBr\}$), hydrogen-bonded cycles with an apparent relation to the solid-state structure of the parent aminoalcohol. The X–H···Br hydrogen bonding is further aided with weak intermolecular C(2)–H(2)···O^{v} [3.312(4) Å; (v) $(1-x, 1-y, -z)$] and C(11)–H(11B)···Br [3.769(2) Å] interactions.

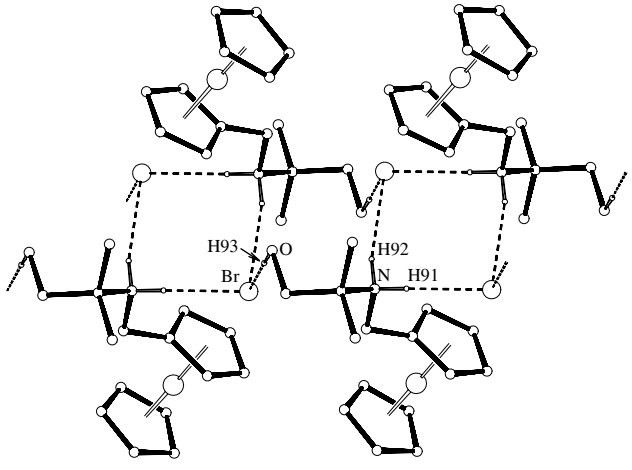

Fig. 3. A view of the hydrogen-bonded chains in the structure of **2**.

2.3. Solid-state structure of *3a*

The monoclinic unit cell of **3a** contains three crystallographically independent $[\mathbf{1}H][H_2PO_4]$ ion pairs and extensively disordered molecules of solvating diethyl ether, which were refined to sum up to two molecules per the unit cell. Similarly to **2**, the protonation results in a lengthening of the C–N bonds and changes in the conformation of the side chain (cations 1 and 3, Table 2).

Far more interesting in the structure of **3a**, however, is the crystal packing, which differs noticeably from those of **1** and **2**. In the unit cell, there are four infinite hydrogen-bonded dihydrogenphosphate chains running parallel to the crystallographic *a* axis (Fig. 4(a), Table 3). In these chains, each dihydrogenphosphate moiety acts as a double hydrogen bond donor using its two P–O*H* hydrogen atoms and a double hydrogen bond acceptor to two P=*O* oxygen atoms. The cations $[\mathbf{1}H]^+$ are oriented so that their polar ($^+NH_2$ and OH) groups point towards the linear phosphate framework while the nonpolar ferrocene parts are inclined to each other so that they form hexagonal hydrophobic channels, which ac-

Table 2
The pertinent bond distances, bond, torsion and dihedral angles for three crystallographic independent molecule in the structure of **3a** (Å and °)[a]

Molecule (*n*)	**1**	**2**	**3**
Fe–Cg1	1.645(1)	1.652(1)	1.648(1)
Fe–Cg2	1.648(1)	1.658(1)	1.655(1)
C(*n*01)–C(*n*11)	1.494(3)	1.494(3)	1.489(3)
C(*n*11)–N(*n*)	1.509(3)	1.488(3)	1.512(3)
N(*n*)–C(*n*12)	1.521(3)	1.521(3)	1.518(3)
C(*n*12)–C(13)	1.525(3)	1.525(3)	1.522(3)
C(*n*13)–O(*n*)	1.416(3)	1.415(3)	1.421(3)
∠Cp1,Cp2	2.7(1)	2.9(2)	2.9(1)
C(*n*1)–C(*n*11)–N(*n*)	109.4(2)	112.9(2)	109.8(2)
C(*n*11)–N(*n*)–C(*n*12)	117.6(2)	116.4(2)	117.6(2)
N–C(*n*12)–C(*n*13)	108.1(2)	107.5(2)	107.7(2)
C(*n*12)–C(*n*13)–O(*n*)	109.6(2)	107.3(2)	109.1(2)
C(*n*1)–C(*n*11)–N(*n*)–C(*n*12)	−159.4(2)	170.3(2)	154.2(2)

Plane definitions: Cp1, C(*n*01–*n*05); Cp2, C(*n*06–*n*10). Cg1 and Cg2 are the respective ring centroids.

[a] The labelling of the cationic part is analogous to that for neutral **1** with the molecule number added as the first digit (cf. Fig. 1).

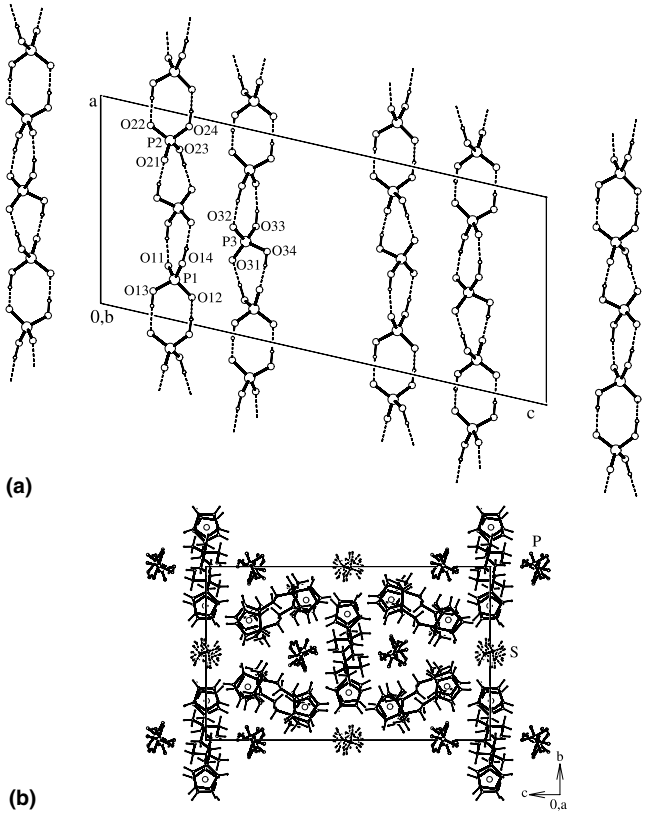

Fig. 4. A view of the unit cell of **2a** along the crystallograhic *c* axis showing (a) only the hydrogen bonded phosphate chains (H bonds are shown as dashed lines) and (b) a projection of the unit cell of **2a** onto the *bc* plane showing the phosphate chains (P) surrounded by a trigonal assembly of the cations, and the solvate occupied channels (S; H bonds not indicated for clarity).

commodate the disordered solvate molecules (channel diameter ca. 5.2 Å; Fig. 4(b)).

Of the three crystallographically independent $[\mathbf{1}H]^+$ cations, two associate into asymmetric hydrogen-bridged dimers via pairs of NH···O bonds similar to the repeating dimeric unit in the structure of free aminoalcohol **1**. However, the N···O distances are significantly different (3.063(3) and 2.850(3) Å), and both shorter than those in **1**-most likely due to being charge-assisted. Besides, all cations feature an additional intramolecular hydrogen NH···O bonding though with quite unvaforable N–H···O angles (102°–107°). The dimeric as well as the "isolated" cation moieties form hydrogen bonds to deprotonated oxygen atoms in the phosphate chains (Table 3), each cation acting as a double hydrogen bond donor from both the OH and NH groups. Thus, the cations cross-link the infinite linear assembly of the phosphate ions into a complicated three-dimensional network. The solid-state assembly of **3** is undoubtedly dictated by hydrogen bonding but it is apparently supported by non-polar interactions (see Fig. 4(b)), which can be exemplified by C–H···π-ring contacts between the C114–H11e bond and the unsubstituted cyclopentadienyl ring of the "third" cation, C(306–310): Cg···C 3.655(3) Å, C–H···Cg 155°.

Table 3
Hydrogen bond parameters for **3a** (Å and °)[a]

D–H···A	D–H	D···A	D–H···A
Phosphate chains			
O13–H81···O22^{i}	0.92	2.589(2)	178
O14–H82···O32	0.94	2.589(2)	175
O23–H83···O31^{ii}	0.94	2.515(2)	177
O24–H84···O12^{iii}	1.00	2.602(2)	167
O33–H85···O11	0.95	2.579(2)	163
O34–H86···O21^{iv}	0.93	2.540(2)	174
Phosphate–cation interactions			
O1–H93···O11	0.96	2.664(2)	171
O2–H96···O34^{iv}	0.91	2.720(2)	175
O3–H99···O21^{v}	0.92	2.646(2)	169
N1–H91···O32^{ii}	0.94	2.721(2)	164
N2–H95···O22^{vi}	0.91	2.708(2)	176
N3–H98···O12^{v}	0.97	2.725(2)	173
Cation–cation interactions			
N1–H92···O3^{vii}	0.92	3.063(3)	151
N3–H97···O1^{v}	0.91	2.850(3)	151
N1–H92···O1 (intra)	0.92	2.734(2)	107
N2–H94···O2 (intra)	0.96	2.670(3)	106
N3–H97···O3 (intra)	0.91	2.761(2)	102

Parameters involving fixed hydrogen atoms are given without estimated standard deviation (see Section 4). Symmetry codes: (i) $(2-x, y+1/2, 1/2-z)$; (ii) $(1-x, y-1/2, 1/2-z)$; (iii) $(2-x, y-1/2, 1/2-z)$; (iv) $(1-x, y+1/2, 1/2-z)$; (v) $(x-1, y, z)$; (vi) $(1-x, 1-y, -z)$; (vii) $(1+x, y, z)$.

[a] D, donor; A, acceptor.

2.4. NMR and electrochemical study

The acid-base behavior and possible ion association of **1** was studied by ^{1}H and ^{31}P NMR spectroscopy in acetonitrile-d_3 solutions at 298 K. The ^{1}H NMR spectrum of pure **1** exhibits only one, combined broad signal due to NH and OH protons. Upon sequential addition of tetrabutylammonium dihydrogenphosphate, the intensity of this combined signal increases proportionally to the amount of added dihydrogenphosphate and the signal shifts progressively to a lower field in the entire range followed ($\Delta\delta_H$ ca. 2 ppm for 0–10 equiv. $H_2PO_4^-$, non-linear). The other resonances are influenced much less: the signals of the methylene groups (NCH_2, OCH_2) and one signal of the substituted cyclopentadienyl ring (α-CH) show significantly less pronounced shifts, attaining constant positions with about 1 equiv. $Bu_4NH_2PO_4$ added, while the remaining signals (Me and C_5H_5) are virtually unaffected. The single resonance observed in $^{31}P\{^1H\}$ NMR spectra behaves similarly to the acidic protons albeit with a much smaller absolute change ($\Delta\delta_P$ ca. 0.17 ppm for 0.25–10 equiv.) and reaches a constant position with ca. 8 equiv. $H_2PO_4^-$.

An addition of up to 5 equiv. Bu_4NBr into a solution of **1** in acetonitrile-d_3 causes no detectable shift of the ^1H resonances, the only observed change being a slight sharpening of the broad signal due to NH/OH protons. Analogous titrations with HBr and H_3PO_4 could not be done because the addition of the acids resulted in the separation of the respective ammonium salts. Nevertheless, a shift of the ^1H NMR resonances similar to the dihydrogenphosphate-**1** system but steeper could be observed clearly upon addition of HBr (in the range of 0–0.5 equiv. HBr). Thus, the changes in the NMR spectra can be accounted predominantly for acid–base equilibria involving the **1**/[**1**H]$^+$ and $H_nPO_4^{(n-3)}$ species, where $n = 0$–3.

The **1**-$H_2PO_4^-$ system was further followed by voltammetry on a rotating platinum disk electrode (RDE) and by cyclic voltammetry (CV) on a stationary platinum disk electrode (Table 4, Figs. 5 and 6). Voltammogram of **1** on RDE exhibits one diffusion controlled wave (Fig. 5(a)) while cyclovoltammogram of **1** displays a couple of peaks clearly attributable to a reversible one-electron ferrocene/ferricenium redox process (Fig. 6(a)). Compared to ferrocene/ferricenium reference, the couple is shifted by 20 mV to more negative potentials, indicating a slight electrondonating nature of the pendant group.

An addition of $Bu_4NH_2PO_4$ into a solution of **1** changes the electrochemical response (Figs. 5(b) and 6(b)–(d)). With an increasing dihydrogenphosphate concentration, the ferrocene oxidation wave (or the couple of the CV peaks) shows a progressive cathodic shift (ca. 20 mV with 1 equiv., and ca. 40 mV with 5 equiv. $H_2PO_4^-$). The cathodic shift of the ferrocene oxidation wave can be explained by an electron density lowering at iron atom upon protonation of the side chain, with a possible synergism of an adduct formation. A rather low magnitude of the shift corresponds with the presence of a non-conjugated (methylene) spacer between the reaction center and the redox unit.

Upon addition of dihydrogenphosphate, the voltammograms on RDE loose their characteristic sigmoidal shape (Fig. 5(a)) and the current starts to decline before reaching the original limiting value (Fig. 5(b)). Repeating of the voltammetric scan without cleaning the electrode results in a yet lower maximum current. Such a behavior indicates a formation of a film on the electrode surface [9], which partly prevents the electrode processes. The cyclic voltammograms are also changed: the newly emerged anodic pre-peak and the second cathodic peak at more negative potentials (Fig. 6(b)–(d)) are most likely due to oxidation and reduction of the adsorbed species, respectively. The simultaneous increase of the anodic/cathodic peak separation with increasing concentration of $H_2PO_4^-$ corresponds to the fact that the kinetics of the electron transfer through the growing film on the electrode surface is slower and the system becomes quasi-reversible. The mentioned effects are even more pronounced when the potential of the electrode is set for several seconds at +0.35 V to remove the passivating material and diminish upon repeated cycling.

Table 4
Electrochemical data[a]

System	E_{pa} (V)	E_{pc} (V)	$E_{1/2}$ (V)
1	+0.01	−0.05	0.02[b]
1 + 1/2 $Bu_4NH_2PO_4$	+0.01	−0.05	
1 + 1 $Bu_4NH_2PO_4$	−0.01	−0.08	
1 + 5 $Bu_4NH_2PO_4$	−0.03	–	

[a] In acetonitrile on platinum disk electrode. The potentials are given relative to ferrocene/ferricenium couple. Parameters of the sorption peaks are not given.

[b] $E_{1/2}$ values for **1** obtained from voltammetry and CV are identical.

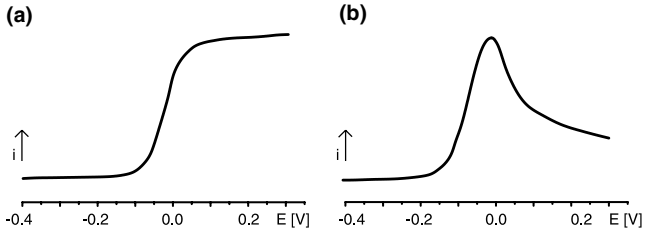

Fig. 5. Voltammograms of **1** on platinum RDE before (a) and after (b) addition of one molar equivalent of $Bu_4NH_2PO_4$ (see Section 4 for details).

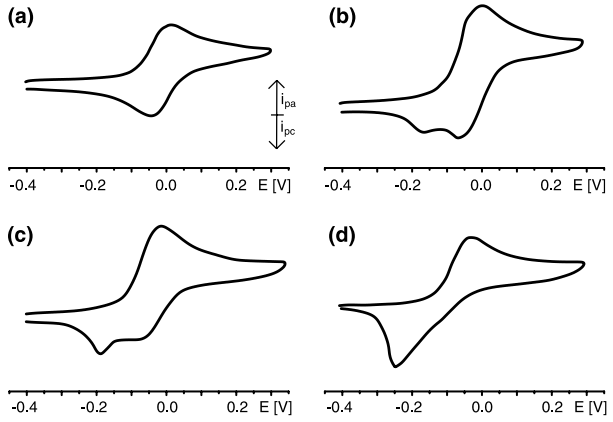

Fig. 6. Cyclic voltammograms of compound **1** without (a) and after addition of 0.5 (b), 1 (c) and 5 (d) equiv. $Bu_4NH_2PO_4$. The potentials are given relative to ferrocene/ferricenium couple. For experimental details see Section 4.

3. Conclusions

Aminoalcohol **1** can be considered a new entry among organometallic building blocks for the preparation of self-assembled crystalline materials. It combines the rigid, redox-active ferrocene unit with conformationally adaptable β-hydroxyamine side chain and can be easily converted to ammonium salts, solid-state packing of which, as exemplified for **2** and **3**, seems to be controlled

in a large extent by the counter ion properties (polarizability and hydrogen bonding ability). Besides such a structural variability, the use of $[\mathbf{1}H]^+$ salts is advantageous over neutral molecules due to a charge-support to hydrogen bonding (see, for instance, charge-assisted H-bonding in ammonium ferrocene carboxylates [10a] and ferrocenylpyridium salts [10b]).

4. Experimental

4.1. General comments

Chloroform was dried by standing over potassium carbonate and methanol was freshly distilled from a sodium methoxide solution. Other reagents were used as received from commercial suppliers. The syntheses were performed with exclusion of a direct sun light.

NMR spectra were recorded on a Varian UNITY Inova 400 spectrometer (^{1}H, 399.95; ^{13}C, 100.58 MHz) at 298 K. Chemical shifts (δ/ppm) are given relative to internal tetramethylsilane (^{1}H, ^{13}C) and external 85% aqueous H_3PO_4 standards. In NMR titrations, aliquots of 0.2 M $Bu_4NH_2PO_4$ in CD_3CN were sequentially added into a 0.02 M solution of **1** in the same solvent (0.6 ml) using a calibrated microsyringe. ^{1}H and ^{31}P{^{1}H} NMR spectra were measured immediately after careful mixing. ^{1}H spectrum recorded for a solution of **1** (0.6 ml 0.02 M) diluted with acetonitrile-d_3 to the same final volume (1.2 ml) showed no difference compared to the spectrum of the undiluted sample, indicating that the chemical shift of the NH/OH protons is independent of the concentration in the studied range. The titrations with Bu_4NBr, HBr and H_3PO_4 were performed similarly (0.2 M solution of the acids were prepared by dilution of concentrated aqueous solutions with CD_3CN).

IR spectra were recorded on an FT IR Nicolet Magna 650 instrument in the range of 400–4000 cm^{-1}. Electron impact mass spectra (EI MS) were measured on a Finnigan MAT INCOS 50 mass spectrometer interfaced to a Varian 3400 gas chromatograph equipped with an SPB-5 capillary column (He carrier gas, injector temperature 250 °C). The spectra were acquired at electron energy 70 eV. Melting points are uncorrected.

Electrochemical measurements were performed on a multipurpose polarograph PA3 interfaced to an XY Recorder 4103 (Laboratorní přístroje, Prague) at room temperature under argon blanket using a standard three-electrode system: platinum disk working electrode (diameter 2 mm), a platinum wire auxiliary electrode and saturated calomel reference electrode separated from the analyzed solution by a bridge filled with a Bu_4NPF_6 solution in acetonitrile to ensure an exclusion of water and, typically, 5×10^{-4} M solutions of **1** in acetonitrile (International Enzymes, $\geqslant$99%) containing 0.05 M Bu_4NPF_6 (Fluka, purriss.) as the base electrolyte and an appropriate amount of $Bu_4NH_2PO_4$ added as a 0.05 M solution by a microsyringe. Voltammograms were recorded on a rotating disk electrode (RDE; 1000 min^{-1}) with the scan rate of 50 mV s^{-1} and the cyclic voltammograms on the stationary electrode at the scan rate of 100 mV s^{-1}. The potentials are given in volts relative to the redox potential of the ferrocene/ferricenium standard.

4.2. Synthesis of 2-(ferrocenylmethyl)amino-2-methylpropan-1-ol (*1*)

Ferrocenecarboxaldehyde (428.9 mg, 2.00 mmol) and 2-amino-2-methylpropan-1-ol (188.1 mg, 2.10 mmol) were dissolved in dry chloroform (20 ml) and the solution was refluxed for 3 h under an argon atmosphere. Then, the solvent was removed under reduced pressure and the dark, rusty brown residue (δ_H 8.18, C*H*=N of the imine intermediate) was dissolved in dry methanol (20 ml). The solution was cooled in an ice bath and sodium tetrahydridoborate (378 mg, 10 mmol) was slowly introduced. After stirring for 1 h at 0 °C and for another 3 h at room temperature, the reaction was terminated by addition of aqueous sodium hydroxide solution (20 ml 10%) and the yellow mixture was extracted with dichloromethane. The combined extracts were washed with saturated aqueous sodium chloride solution, dried over magnesium sulfate and evaporated under vacuum. The yellow residue was purified by chromatography on a short silica gel column using ethyl acetate to remove ferrocenylmethanol (yellow solid; 43 mg, 10%) and then ethyl acetate-methanol mixtures with methanol content gradually increasing up to 50% to elute aminoalcohol **1**. Evaporation of the second fraction, redissolving in little ethyl acetate, filtration and solvent removal under vacuum afforded pure **1** as a rusty orange solid (414.0 mg, 72%).

M.p. 114–116 °C. NMR ($CDCl_3$): δ_H 1.12 (s, 6 H, C*Me*$_2$), 3.31, 3.38 (2×s, 2 H, FcC*H*$_2$ and C*H*$_2$O); 4.10 (apparent t, 2 H, C$_5$*H*$_4$), 4.13 (s, 5 H, C$_5$*H*$_5$), 4.19 (apparent t, 2 H, C$_5$*H*$_4$); δ_C 24.20 (C*Me*$_2$), 40.95 (Fc*C*H$_2$), 53.66 (*C*Me$_2$), 67.68, 67.93 (C$_5$H$_4$, *C*H); 68.35 (*C*H$_2$O), 68.39 (*C*$_5$H$_5$), 87.79 (C$_5$H$_4$, *C*$_{ipso}$). IR (Nujol): ν/cm^{-1} ν_{OH}, ν_{NH} 3273 vs, ca. 3158 br composite; 1106 s, 1081 s, 1066 vs, 1025 s, 996 m, 853 s, 811 vs, 507 m, 456 s, 490 m. EI MS: *m*/*z* (relative abundance) 288 (3), 287 (20, $M^{+\cdot}$), 200 (13), 199 (100, "[FcCH$_2$]$^+$"), 197 (6), 186 (3, FcH$^{+\cdot}$), 128 (4), 122 (4), 121 (36, [C$_5$H$_5$Fe]$^+$), 78 (6), 58 (5), 56 (17, Fe$^+$), 42 (5), 39 (3). *Anal.* Calc. for $C_{15}H_{21}FeNO$: C, 62.73; H, 7.37; N, 4.88. Found: C, 62.72; H, 7.44; N 4.84%.

4.3. Preparation of (ferrocenylmethyl)(3-hydroxy-2-methylprop-2-yl)ammonium bromide (*3*)

In an intended NMR titration, a solution of aminoalcohol **1** (0.02 M) in acetonitrile-d_3 (0.60 ml) was

treated sequentially with 0.2 M HBr in the same solvent (prepared by diluting 47% aqueous acid). After addition of a half molar equivalent (30 μl), separation of yellow microcrystalline salt **3** started. Finally, up to 1 molar equivalent of the acid was added (total 60 μl) and, after standing for several hours, the crystalline solid was filtered off, dried in air, and used directly for X-ray structure determination. The yield was not determined. Positive-ion ESI (Bruker Esquire 3000, dissolved in MeOH): *m/z* 199 (base peak, "$[FcCH_2]^+$"), 288 ($[\mathbf{1}H]^+$), 655 and 657 (weak, $[(\mathbf{1}H)_2Br]^+$, ^{79}Br and ^{81}Br isotopomers).

4.4. Synthesis of (ferrocenylmethyl)(3-hydroxy-2-methylprop-2-yl)ammonium dihydrogenphosphate (2)

Aminoalcohol **1** (143.6 mg, 0.50 mmol) was dissolved in methanol (5 ml), and the solution treated with 85% aqueous phosphoric acid (35 μl, ca. 0.55 mmol). After standing at room temperature overnight, the product was precipitated by addition of diethyl ether (ca. 30 ml). The precipitate was filtered off, washed with diethyl ether and dried in air at 80 °C for 30 min. Yield: 190.1 mg (99%), yellow solid.

NMR (CD_3OD): δ_H 1.32 (s, 6 H, C*Me*$_2$), 3.59, 3.97 (2×s, 2 H, C*H*$_2$); 4.23 (s, 5 H, C$_5$*H*$_5$), 4.28, 4.40 (2×s, 2 H, C$_5$*H*$_4$); δ_C 21.36 (C*Me*$_2$), 42.70 (*C*Me$_2$), 60.06, 65.91 (2×*C*H$_2$); 70.00 (*C*$_5$H$_5$), 70.46, 71.39 (C$_5$H$_4$, *C*H); 78.65 (C$_5$H$_4$, *C*$_{ipso}$); δ_P 2.6 (s, phosphate). IR (Nujol): *ν*/cm^{-1} ν_{OH}, ν_{NH} 3363 br m, 3212 w, ≈3140 br m, 3103 w, 3081 w, 3078 w, 2380 s br; 1618 m, 1591 w, 1286 w, 1249 m, 1231 m, $\nu_3(PO_4)$ 1105–1044 s composite; $\nu_1(PO_4)$ 971–942 s composite; 898 w, 843 m, 805 m, ≈538 m, 513 s, 487 m, 454 m. *Anal*. Calc. for $C_{15}H_{24}FeNO_5P$: C, 46.77; H, 6.28; N, 3.64. Found: C, 46.95; H, 6.63; N 3.63%.

4.5. X-ray crystallography

X-ray quality crystals of **1** (orange bar, 0.20 × 0.20 × 0.43 mm^3), **3a** (yellow orange needle, 0.08 × 0.10 × 0.50 mm^3) were obtained by recrystallization from methanol and by diffusion of diethyl ether into a methanol solution of **3**, respectively. Microcrystalline **2** was obtained from the NMR experiment (yellow prism, 0.05 × 0.06 × 0.10 mm^3).

Full-set diffraction data ($\pm h \pm k \pm l$) for all compounds were collected on an Nonius KappaCCD diffractometer equipped with Cryostream Cooler (Oxford Crysoystems) at 150 K using graphite monochromatized Mo Kα radiation ($\lambda = 0.71073$ Å) and analyzed with HKL program package [11].

Crystallographic data for ***1***: $C_{15}H_{21}FeNO$ (M = 287.18 g mol^{-1}), monoclinic, space group $P2_1/c$ (no. 14), $a = 5.6705(1)$, $b = 19.3315(4)$, $c = 12.1647(2)$ Å; $\beta = 94.974(1)°$, $V = 1328.46(4)$ Å^3, $Z = 4$, $\rho_{calc} = 1.436$ g cm^{-3}, $F(000) = 608$; $2\theta_{max} = 55°$, 5828 total, 3030 unique ($R_{int} = 2.7\%$), 2684 observed [$I > 2\sigma(I)$] diffractions; 156 parameters. Cell parameters were determined by least-squares analysis from 40 802 partial diffractions with $1.0 \leqslant \theta \leqslant 27.5°$. Absorption was neglected [μ(Mo Kα) = 1.122 mm^{-1}].

Crystallographic data for ***2***: $C_{15}H_{22}BrFeNO$ (M = 368.10 g mol^{-1}), triclinic, space group $P\bar{1}$ (no. 2), $a = 7.6548(2)$, $b = 10.3098(5)$, $c = 10.5700(4)$ Å; $\alpha = 109.071(2)$, $\beta = 91.969(2)$, $\gamma = 101.505(2)°$, $V = 768.08(5)$ Å^3, $Z = 2$, $\rho_{calc} = 1.592$ g cm^{-3}, $F(000) = 376$; $2\theta_{max} = 55°$, 12 988 total, 3495 unique, 2730 observed [$I > 2\sigma(I)$] diffractions; 172 parameters. Cell parameters were determined by least-squares analysis from 3334 partial diffractions with $1.0 \leqslant \theta \leqslant 27.5°$. Numerically corrected for absorption [μ(Mo Kα) = 3.575 mm^{-1}], transmission coefficient range: 0.839–0.865.

Crystallographic data for ***3a***: $C_{15}H_{24}FeNO_5P \cdot 1/6(C_4H_{10}O)$ (M = 397.53 g mol^{-1}), monoclinic, space group $P2_1/c$ (no. 14), $a = 12.4617(2)$, $b = 16.3022(1)$, $c = 27.4132(3)$ Å; $\beta = 102.8566(6)°$, $V = 5429.5(1)$ Å^3, $Z = 12$, $\rho_{calc} = 1.459$ g cm^{-3}, $F(000) = 2508$; $2\theta_{max} = 52°$, 20 845 total, 10 681 unique, 8860 observed [$I > 2\sigma(I)$] diffractions; 652 parameters. Cell parameters were determined by least-squares analysis from 61 640 partial diffractions with $1.0 \leqslant \theta \leqslant 26.0°$. Absorption was neglected [μ(Mo Kα) = 0.947 mm^{-1}].

The structures were solved by direct methods (SIR92 [12]) and refined by weighted full-matrix least squares procedure on F^2 (SHELXL97 [13]). The final geometric calculations were carried out with PLATON program [14]. Particular details of the structure solution follow:

1: difference electron density maps revealed a disorder in the unsubstituted cyclopentadienyl ring. The ring was modelled as if being contributed from two mutually rotated, regular pentagons (C–C 1.40 Å) with fractional occupancies of 0.60 (A) and 0.40 (B) and anisotropic thermal motion parameters restrained to identical values in each C*n*A–C*n*B pair (n = 6–10). All non-hydrogen atoms were refined with anisotropic thermal motion parameters. Hydrogen atoms at the amine and hydroxy groups were identified on difference density maps and freely isotropically refined. All other hydrogen atoms were included in calculated positions [C–H bond lengths 0.97 (methylene), 0.96 (methyl), and 0.93 (aromatic) Å] and assigned $U_{iso}(H) = 1.2\ U_{eq}(C)$ (methylene, and aromatic) or 1.5 U_{eq}(C) (methyl). Final R indices; observed (all) diffractions: R 4.38% (5.20%), wR 9.03% (9.34)%. Extremes on the final difference electron density map: +0.79, −0.56 e Å^{-3}.

2: All non-hydrogen atoms were refined with anisotropic thermal motion parameters. Hydrogen atoms at the nitrogen and oxygen atoms were fixed in the positions revealed by difference electron density maps and assigned $U_{iso}(H) = 1.5\ U_{eq}(X)$, X = N or O. Aromatic, methyl and methylene hydrogen atoms were treated as above. Final R indices; observed (all) diffractions: R

3.33% (5.24%), *wR* 6.45% (7.11)%. Extremes on the final difference electron density map: +0.94, −0.54 e Å^{-3}.

3a: All non-hydrogen atoms were refined anisotropically. Hydrogen atoms at the ammonium, hydroxy, and phosphate groups were included in the positions revealed by difference density maps and assigned a fixed isotropic thermal motion parameter. Aromatic, methyl and methylene hydrogen atoms were treated as for **1**. Final *R* indices; observed (all) diffractions: *R* 3.50% (4.74%), *wR* 8.58% (9.05)%. Extremes on the final difference electron density map: +0.67, −0.51 e Å^{-3}.

5. Supplementary data

Crystallographic data excluding structure factors have been deposited with the Cambridge Crystallographic Data Centre [Deposition Nos. CCDC-200996 (**1**), −200997 (**2a**), and −213707 (**3**)]. Copies of the data may be obtained upon request to CCDC, 12 Union Road, Cambridge CB2 1EZ, UK; http://www.ccdc.cam.ac.uk, e-mail: deposit@ccdc.cam.ac.uk.

Acknowledgements

This research was supported by Grant Agency of the Czech Republic (Grant Nos. 203/01/P002 and 203/99/M037) and is a part of a long-term Research plan of the Faculty of Sciences, Charles University. We thank Mr. T. Baše for assistance at early stages of this work and Dr. M. Štícha for GC–MS measurements.

References

[1] (a) D. Braga, F. Grepioni, A.G. Orpen (Eds.), Crystal Engineering: From Molecules and Crystals to Materials, Kluwer Academic Publishers, Dordrecht, 1999;
(b) D. Braga, F. Grepioni, G.R. Desiraju, Chem. Rev. 98 (1998) 1375;
(c) D. Braga, F. Grepioni, J. Chem. Soc., Dalton Trans. (1999) 1;
(d) D. Braga, J. Chem. Soc., Dalton Trans. (2000) 3705;
(e) D. Braga, F. Grepioni, Chem. Commun. (1996) 571.

[2] (a) G.A. Jeffrey, An Introduction to Hydrogen Bonding, Oxford University, New York, 1997;
(b) G.R. Desiraju, T. Steiner, The Weak Hydrogen Bond in Structural Chemistry and Biology, Oxford University, New York, 1999;
(c) T. Steiner, Angew. Chem., Int. Ed. 41 (2002) 48.

[3] (a) C. Glidewell, R.B. Klar, P. Lightfoot, C.M. Zkaria, G. Ferguson, Acta Crystallogr., Sect. B 52 (1996) 110;
(b) G. Ferguson, J.F. Gallagher, C. Glidewell, C.M. Zakaria, Acta Crystallogr., Sect. C 49 (1993) 967;
(c) G. Ferguson, J.F. Gallagher, C. Glidewell, C.M. Zakaria, J. Organomet. Chem. 464 (1994) 94;
(d) P. Štěpnička, T. Baše, Inorg. Chem. Commun. 4 (2001) 682;
(e) P. Štěpnička, I. Císařová, New J. Chem. 26 (2002) 1389;
(f) G. Ferguson, C. Glidewell, G. Opromolla, C.M. Zakaria, P. Zanello, J. Organomet. Chem. 517 (1986) 183;
(g) R.A. Bartsch, P. Kus, R.A. Holwerda, B.P. Czech, X. Kou, N.K. Dalley, J. Organomet. Chem. 522 (1996) 9.

[4] (a) G. Ferguson, J.F. Gallagher, C. Glidewell, C.M. Zakaria, J. Chem. Soc., Dalton Trans. (1993) 3499;
(b) C. Glidewell, G. Ferguson, A.J. Lough, C.M. Zakaria, J. Chem. Soc., Dalton Trans. (1994) 1971;
(c) C.M. Zakaria, G. Ferguson, A.J. Lough, C. Glidewell, Acta Crystallogr., Sect. C 58 (2002) m1;
(d) C.M. Zakaria, G. Ferguson, A.J. Lough, C. Glidewell, Acta Crystallogr., Sect. C 58 (2002) m5 (only recent and representive examples).

[5] A. Hess, O. Brosch, T. Wyehermueller, N. Metzler-Nolte, J. Organomet. Chem. 589 (1999) 75.

[6] In another experiment, anhydrous magnesium sulfate was added to a solution of ferrocenecarboxaldehyde and the aminoalcohol in dichloromethane in order to promote Schiff base formation. After short stirring, the drying agent was removed and the filtrate evaporated. A subsequent reduction ($NaBH_4$/methanol) gave **1** in 46% isolated yield along with a considerable amount of ferrocenemethanol. T. Baše, P. Štěpnička, unpublished results.

[7] T. Baše, I. Císařová, P. Štěpnička, Inorg. Chem. Commun. 5 (2002) 46.

[8] D. Mootz, D. Brodalla, M. Wiebcke, Acta Crystallogr., Sect. C 45 (1989) 754.

[9] The surface of the electrode may be blocked by (electrogenerated) adducts or materials resulting from a decomposition of the ferrocenium species.

[10] (a) D. Braga, L. Maini, F. Paganelli, E. Tagliavini, S. Casolari, F. Grepioni, J. Organomet. Chem. 637–639 (2001) 609;
(b) D. Braga, M. Polito, M. Bracaccini, D. D'Addario, E. Tagliavini, L. Sturba, F. Grepioni, Organometrallics 22 (2003) 2142.

[11] Z. Otwinowski and W. Minor, HKL Denzo and Scalepack program package by Nonius BV, Delft, 1997. For a reference see: Z. Otwinowski, W. Minor, Methods Enzymol. 276 (1997) 307.

[12] A. Altomare, M.C. Burla, M. Camalli, G. Cascarano, C. Giacovazzo, A. Guagliardi, G. Polidori, J. Appl. Cryst. 27 (1994) 435.

[13] G.M. Sheldrick, SHELXL97. Program for Crystal Structure Refinement from Diffraction Data, University of Göttingen, Göttingen, Germany, 1997.

[14] A.L. Spek, PLATON – a multipurpose crystallographic tool, 2001. Available from: <http://www.cryst.chem.uu.nl/platon/>.